Chinese Chemical Letters 36 (2025) 110109

Contents lists available at ScienceDirect

Chinese Chemical Letters

journal homepage: www.elsevier.com/locate/cclet

Precise assessment of lung cancer-derived exosomes based on dual-labelled membrane interface

Lingjun Sha[a,1], Bing Bo[b,1,*], Jiayu Li[b], Qi Liu[a], Ya Cao[a,*], Jing Zhao[a,*]

[a] Center for Molecular Recognition and Biosensing, Shanghai Engineering Research Center of Organ Repair, School of Life Sciences, Shanghai University, Shanghai 200444, China
[b] Department of Medical Oncology, Shanghai Pulmonary Hospital & Thoracic Cancer Institute, Tongji University School of Medicine, Shanghai 200433, China

ARTICLE INFO

Article history:
Received 25 March 2024
Revised 30 April 2024
Accepted 11 June 2024
Available online 12 June 2024

Keywords:
Lung cancer-derived exosome
Programmed death ligand-1
DNA assembly reaction
Ratiometric signal
Electrochemical analysis

ABSTRACT

Lung cancer-derived exosomes are a kind of valuable and clinically-predictable biomarkers for lung cancer, but they have the limitations in individual differences when being applied in liquid biopsy. To improve their application value and accuracy in clinical diagnosis, a dual-labelled electrochemical method is herein reported for precise assessment of lung cancer-derived exosomes. To do so, two probes are prepared for the dual labeling of exosome membrane to run DNA assembly reactions: One is modified with cholesterol and can insert into exosome membrane through hydrophobic interaction; another one is linked with programmed death ligand-1 (PD-L1) antibody and can bind to exosome surface-expressing PD-L1 *via* specific immunoreaction. Quantum dots-tagged signal strands are used to collect respective DNA products, and produce stripping signals corresponding to the amounts of total exosome and surface-expressing PD-L1, respectively. A wide linear relationship is established for the quantitative determination of lung cancer-derived exosomes in the range from 10^3 to 10^{10} particles/mL, whereas the ratiometric value of the two stripping signals is proven to have a better diagnostic use in screening and staging of lung cancer when being applied to clinical samples. Therefore, our method might provide a new insight into precise diagnosis of lung cancer, and offer sufficient information to reflect the biomarker level and guide the personalized treatment level even at an early stage in clinic.

Lung cancer, a global high-incidence tumor, is usually diagnosed at an advanced stage and associated with poor outcome and a relatively low five-year survival rate [1]. This is primarily due to the limitations of screening techniques [2,3]. For example, computerized tomography, the most commonly used approach for early screening of lung cancer, is accompanied by a high risk of radiation exposure; while tissue biopsy, the "gold standard" approach for pathological examination of lung cancer, has the disadvantages of low sensitivity and a potential risk of distant metastasis. In view of this, a non- or minimally-invasive technology, liquid biopsy, is now gaining considerable attention in dynamic monitoring of the malignant disease from the point of diagnosis to therapy [4,5]. As a typical kind of biomarkers in liquid biopsy, lung cancer-derived exosomes, the membrane-containing vesicles carrying abundant biological substances from the tumor of the origin, have been found to be highly valuable and clinically-predictable [6-8]. Lung cancer-derived exosomes participate in the whole processes of tumor occurrence and development, and their levels are usually elevated in patients in comparison to healthy people [9,10]. Therefore, accurate analysis of lung cancer-derived exosomes is of great importance for early screening and diagnosis of lung cancer.

Over the last decade, impressive progresses have been made on exosome analysis in lung cancer [11-16]. However, a majority of existing methods are constructed depending on universal biomarkers at the exosome surface (*e.g.*, CD9, CD63, and CD81), and have some drawbacks in practical use. On one hand, the methods using universal biomarkers are directed to the total amount of circulating exosomes, which not only contain cancer-derived exosomes but also inevitably contain other exosomes shed by normal cells. On the other hand, exosome secretion comprises a series of complex biological processes and is affected by various factors, and thus circulating exosome or even cancer-derived exosome level may vary from people to people. In this sense, exosome levels determined relying on the universal biomarker, are not stable cross individuals and may be insufficient to reflect the differences between lung cancer patients and healthy people and fail in tumor staging in cancer diagnosis.

* Corresponding authors.
E-mail addresses: 1986042@qq.com (B. Bo), conezimint@shu.edu.cn (Y. Cao), jingzhao@t.shu.edu.cn (J. Zhao).
[1] These authors contributed equally to this work.

https://doi.org/10.1016/j.cclet.2024.110109
1001-8417/

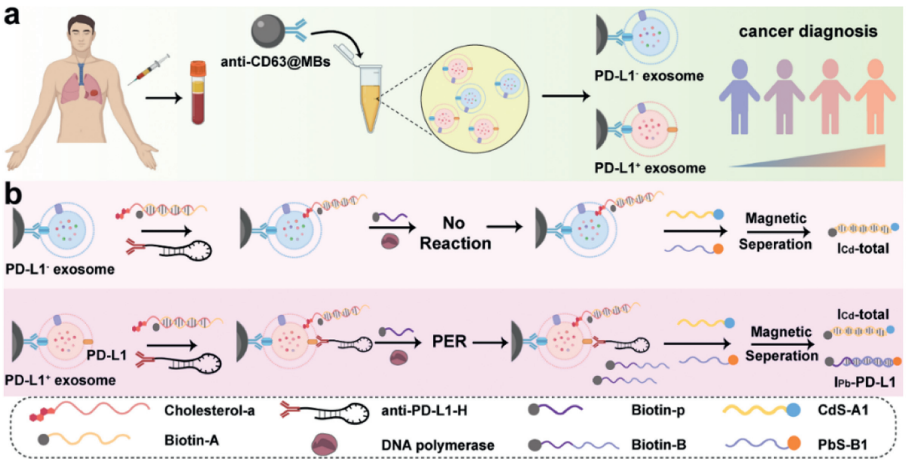

Fig. 1. Schematic illustration of precise assessment of lung cancer-derived exosomes based on the dual-labelled membrane interface.

To address the problem, we herein report a dual-labelled membrane interface-based electrochemical method for precise evaluation of lung cancer-derived exosomes by using both CD63 and programmable death ligand-1 (PD-L1) as exosomal biomarkers. Specifically, CD63 is used as a universal biomarker; and PD-L1, which displays an increased exosomal level with the worse outcome and response to immunotherapy in non-small cell lung cancer is utilized as a tumor-specific biomarker for better understanding of lung cancer. PD-L1 can inhibit the activity of T cells by binding to programmed cell death receptor 1 (PD-1) to enhance tumor immune tolerance. The presence of exosomal PD-L1 is associated with the occurrence of non-small cell lung cancer and the disease progression during immunotherapy treatment. This highlights the potential of exosomal PD-L1 as a biomarker for detecting non-small lung cancer at an early stage and predicting the response to immunotherapy [17-19]. Fig. 1 depicts the principle and workflow of the method. CD63 is first used to enrich exosomes onto CD63 antibody-functionalized magnetic beads (anti-CD63@MBs). Two DNA probes are then prepared to label the membrane of enriched exosomes. One is a cholesterol-modified DNA probe, cholesterol-a/biotin-A, which is able to insert into the exosome membrane through hydrophobic interaction of cholesterol and phospholipid [20]; another one is a PD-L1 antibody-nucleic acid probe, anti-PD-L1-H, which could specially bind to surface-expressing PD-L1. These two probes subsequently participate in two independent DNA assembly reactions, and couple with two quantum dots-tagged signal strands (CdS-A1 and PbS-B1). On one hand, the nucleic acid part (H) of anti-PD-L1-H acts as a catalytic hairpin to trigger a primer exchange reaction (PER) and leads to the programmable extension of a biotin-labeled primer, biotin-p [21]. Thereafter, the extended product, biotin-B, further hybridizes with PbS-B1 to produce a duplex DNA product, PbS-B1/biotin-B. On the other hand, cholesterol-a/biotin-A reacts with CdS-A1 directly, and produces another duplex DNA product, CdS-A1/biotin-A, *via* a strand displacement reaction. Both duplex DNA products (CdS-A1/biotin-A and PbS-B1/biotin-B) are finally enriched by streptavidin-functionalized MBs, and produce stripping signals of Cd and Pb to obtain quantitative information of total exosome and surface-expressing PD-L1, respectively. On this basis, a ratiometric signal is recruited as a quantitative index to reflect the variation in PD-L1 expressions at the exosome level.

To study the feasibility of the method, exosomes collected from a lung cancer cell line NCI-H1299 were used for proof-of-concept studies. Transmission electron microscope image and nanoparticle tracking analysis proved a typical bilayer membrane structure with the mean size of 131 ± 41 nm (Figs. S1 and S2 in Supporting information). Flow cytometry analysis and fluorescence observation demonstrated the positive expression of CD63 at NCI-H1299-derived exosomes and normal exosomes derived from lung cell BEAS-2B, and positive expression of PD-L1 only at exosomes derived from NCI-H1299 (Figs. S3 and S4 in Supporting information). Next, we prepared a FAM-labeled cholesterol-modified DNA probe, cholesterol-a/FAM-A, and proved its successful insertion into the exosome membrane (Fig. S5 in Supporting information). Flow cytometry analysis of the exosome-enriched MBs was also conducted to reconfirm the binding of cholesterol-a/FAM-A to the exosomes through an obvious shift in FAM signal (Fig. S5). Then, fluorescence spectrum was used to characterize the reaction between the cholesterol-modified DNA probe and signal strand A1. As shown in Fig. S6 (Supporting information), low fluorescence was observed in the supernatant after magnetic separation of anti-CD63@MBs that were enriched with NCI-H1299-derived exosomes (NCI-exo@anti-CD63@MBs) and labeled by cholesterol-a/FAM-A (curve a). In contrast, substantial increase of fluorescence intensity was observed in the supernatant of the MBs with further incubation of A1 (curve b), indicating the release of duplex DNA products FAM-A/A1, which proved our design. Furthermore, we prepared Cy3-labled anti-PD-L1-H and verified its binding to surface-expressing PD-L1 through the fluorescence microscopy observation and flow cytometry analysis (Fig. S7 in Supporting information). On this basis, we studied the PER process using the nucleic acid part (H) of anti-PD-L1-H as a catalytic hairpin (Fig. S8A in Supporting information). Fig. S8B (Supporting information) shows polyacrylamide gel electrophoresis analysis of the PER process. Lanes 1–3 displayed the band of PER product B, H, and the hybridization duplex of H and primer p, respectively. Emerged band of B in lane 4 proved the occurrence of PER by using H as the template. Fig. S9 (Supporting information) shows fluorescence spectra of the supernatant after magnetic separation of exosome-enriched MBs to characterize the PER at exosome surface using a FAM-labeled primer (FAM-p) and a quencher-labeled signal strand (BHQ-B1). For PD-L1-experssing NCI-H1299-derived exosomes, extremely low fluorescence was observed undergoing the complete process of PER (curve a) whereas much higher fluorescence was observed in the absence of DNA polymerase (curve b). The experiment was also performed using PD-L1 negative ($PD\text{-}L1^{-}$) BEAS-2B-derived exosomes. As can be seen, despite the presence of DNA polymerase, high fluorescence was observed in this case (curve c). The results were reasonable. FAM-p triggered PER at PD-L1-expressing exosomes and the produced FAM-B hybridized with BHQ-B1 to quench the fluorescence. However, without DNA polymerase or without the expression of PD-L1,

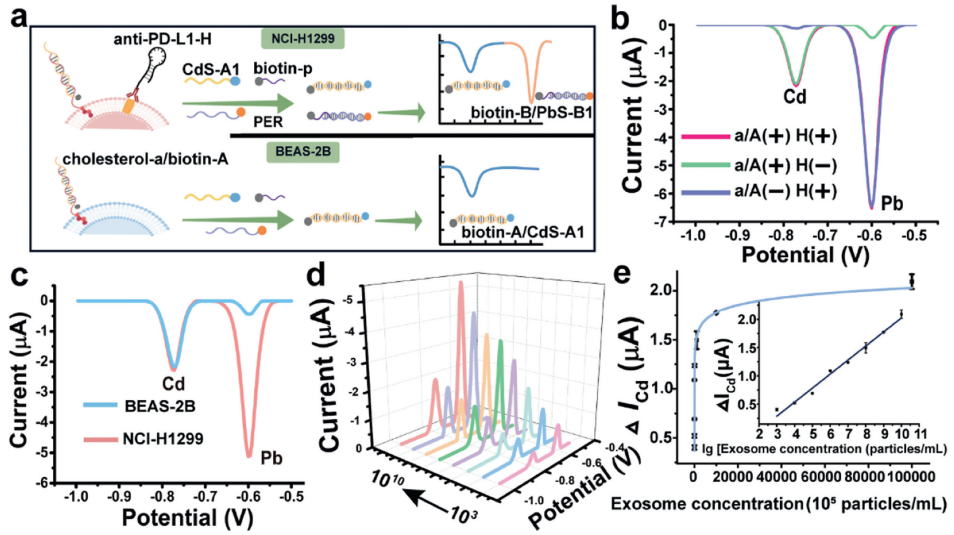

Fig. 2. (a) The workflow for the electrochemical analysis of exosomes. (b) Electrochemical responses with the input of different DNA probes at PD-L1-expressing exosomes. Probes a/A and H represented the cholesterol-a/biotin-A and anti-PD-L1-H, respectively. (c) Electrochemical responses obtained with the addition of exosomes derived from NCI-H1299 or BEAS-2B (10^{10} particles/mL). (d) Electrochemical responses for different concentrations of NCI-H1299-derived exosomes from 10^3 to 10^{10} particles/mL. (e) The relationship between ΔI_{Cd} and the exosome concentrations and the linear relationship between ΔI_{Cd} and the logarithmic values of exosome concentrations (inset).

FAM-p could not be extended to hybridize with BHQ-B1, and thus maintained the intense fluorescence in the supernatant.

Fig. 2a schematically illustrates the workflow for the electrochemical analysis. PD-L1-expressing lung cancer-derived exosomes were labelled with both DNA probes and generated dual products (biotin-A/CdS-A1 and biotin-B/PbS-B1); whereas normal exosomes only bound with cholesterol-modified DNA probe and yielded a single product (biotin-A/CdS-A1). After being enriched onto streptavidin-functionalized MBs, quantum dots within the DNA products were dissolved to release a large amount of Cd and Pb ions, which produced significant electrochemical responses using anodic stripping voltammetry (ASV) (Fig. S10 in Supporting information). Figs. S11 and S12 (Supporting information) show the typical electrochemical responses of CdS and PbS quantum dots using ASV. Fig. 2b shows electrochemical responses with the input of different DNA probes at PD-L1-expressing exosomes. High stripping peaks of both Cd and Pb were observed after input of both cholesterol-a/biotin-A and anti-PD-L1-H (red curve). In contrast, a high peak of Cd but a low peak of Pb were observed with the addition of only cholesterol-a/biotin-A (green line), and a low peak of Cd but a high peak of Pb were observed with the addition of only anti-PD-L1-H (purple line). The high peak currents were in line with the labeling of DNA probes onto the exosome membrane, while the quite low signal of Pb in the green line and the quite low signal of Cd in the purple line were ascribed to the unspecific adsorption of PbS-B1 and CdS-A1, respectively. Fig. 2c further displays electrochemical responses obtained at the exosomes derived from NCI-H1299 or BEAS-2B. Stripping peaks of Cd from the insertion of cholesterol-modified probes were comparable to each other at both exosomes, corresponding to the same amount of both exosomes. While, stripping peak of Pb for exosomes derived from NCI-H1299 was much higher than that for normal exosomes derived from BEAS-2B, which was in line with PD-L1 levels at these two exosomes.

Based on the above verification, we proceeded to investigate the performance of the method for quantitative analysis of lung cancer-derived exosomes in buffer solutions. Before this, several experimental conditions, including the reaction time for the incubation of anti-CD63@MB, exosomes, and anti-PD-L1-H, the reaction time for PER, the reaction time for the incubation of cholesterol-a/biotin-A, and the concentration of cholesterol-a/biotin-A have been optimized to ensure high sensitivity (Figs. S13-S16 in Supporting information). Fig. 2d shows electrochemical responses for different concentrations of NCI-H1299-derived exosomes under the optimized conditions. Fig. 2e further reveals the relationship of ΔI_{Cd} and the exosome concentration ($C_{exosome}$), where ΔI_{Cd} was calculated by subtracting the peak currents of blank control from I_{Cd}. A linear relationship between ΔI_{Cd} (μA) and the logarithmic value of $C_{exosome}$ (particles/mL) was obtained in the range from 10^3 to 10^{10} particles/mL. The equation was $\Delta I_{Cd} = 0.249 \times \lg C_{exosome}$ - 0.461 ($R^2 = 0.99$), and the detection limit was calculated to be 826 particles/mL at the signal-to-noise ratio of 3. ΔI_{Pb} was also found to display a linear relationship with the logarithmic value of NCI-H1299-derived exosome concentration (Fig. S17 in Supporting information), and a detection limit of 985 particles/mL was obtained. These results revealed that both Cd and Pb stripping signals could be used for the quantitative analysis of PD-L1-expressing lung cancer-derived exosomes with a lower detection limit and a wider linear range than existing methods (Table S1 in Supporting information) [22-33].

Despite the success in buffer solutions, there are still some difficulties in applying the method to the analysis of lung cancer clinical samples. On the one hand, the Cd signal corresponds to the number of total exosomes rather than just the amount of lung cancer-derived exosomes, and thus may show insufficient specificity in the diagnosis or staging of lung cancer. On the other hand, the Pb signal corresponds to the amount of exosomal PD-L1, which may be influenced by the exosome amount that is different even among lung cancer patients. Therefore, when the Pb signal is applied to the diagnosis and staging of lung cancer, it may cause false negative results in some cases due to limited exosome secretion. In this sense, a ratiometric signal, $\Delta I_{Pb}/\Delta I_{Cd}$, was further recruited as a quantitative index. The signal employed ΔI_{Pb} to present the exosomal PD-L1 expression while ΔI_{Cd} as a built-in correction signal, and hence provided more precise information for lung cancer-derived exosome analysis in clinical samples.

Figs. 3a and b show the ΔI_{Cd} and ΔI_{Pb} obtained with different concentrations of exosomes derived from BEAS-2B and NCI-H1299. ΔI_{Cd} enhanced with the increase of exosome concentration in the presence of both exosomes, and was approximately equal for both exosomes at each concentration. In comparison, although ΔI_{Pb} increased with the concentration of NCI-H1299-derived exo-

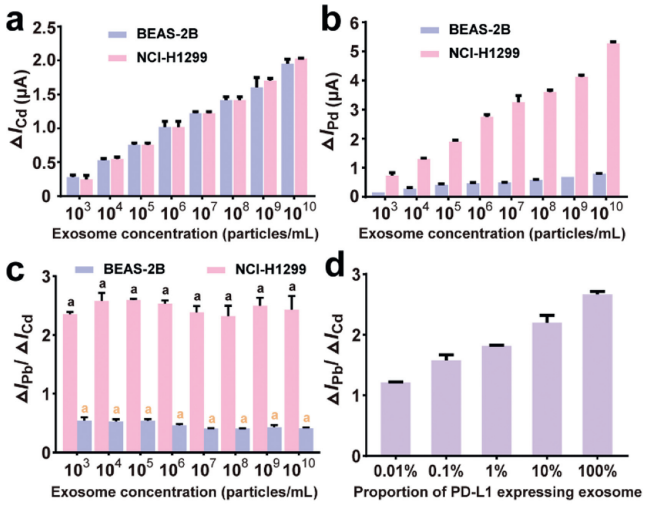

Fig. 3. (a) ΔI_{Cd} and (b) ΔI_{Pb} obtained with different concentrations of normal exosomes derived from BEAS-2B and cancer exosomes derived from NCI-H1299 (From 10^3 to 10^{10} particles/mL). (c) $\Delta I_{Pb}/\Delta I_{Cd}$ obtained with different concentrations of BEAS-2B-derived exosomes and NCI-H1299-derived exosomes. (d) The relationship between the $\Delta I_{Pb}/\Delta I_{Cd}$ and the proportion of PD-L1-expressing exosomes in mixed samples from 0.01% to 100%.

somes, it maintained at a very low level with the normal exosomes even at 10^{10} particles/mL. Fig. 3c displays the $\Delta I_{Pb}/\Delta I_{Cd}$ ratio at different concentrations of the exosomes. Unlike the single signal, the values of $\Delta I_{Pb}/\Delta I_{Cd}$ for either PD-L1-expressing exosomes or normal exosomes displayed no significant differences among varied exosome concentrations. The results not only revealed high internal consistency of both exosomes with stable PD-L1 expression, but also indicated that $\Delta I_{Pb}/\Delta I_{Cd}$ accurately reflected the variation in PD-L1 expression at total exosome level without being affected by the amount of exosomes. To further investigate the usability of the ratiometric signal, we prepared mixed samples containing different proportions of PD-L1-expressing exosomes. As shown in Fig. S18 (Supporting information), ΔI_{Cd} remained steady in all samples, but ΔI_{Pb} enhanced with the increase in the proportion of PD-L1-expressing exosomes. Fig. 3d further reveals the relationship between the $\Delta I_{Pb}/\Delta I_{Cd}$ and the proportion of PD-L1-expressing exosomes in mixed samples. The ratiometric signal was found to increase with the proportion of PD-L1-expressing exosomes and show a linear relationship with the logarithmic value of the proportion (Fig. S19 in Supporting information). These results suggested that the ratiometric signal, although not able to measure the absolute amount of total exosomes or PD-L1-positive exosomes, could stably reflect the variation in PD-L1 expression at the total exosome level.

To prove the potential application of ratiometric signal in clinical diagnosis, the method was adopted to analyze clinical samples. To do so, undiluted serum samples were collected from healthy donors without diseases (HD, $n = 5$) and patients diagnosed with non-small cell lung cancer at the early stages (Stage I&II, $n = 8$) and the advanced stages (Stage III&IV, $n = 11$). The information of clinical samples was listed in Table S2 (Supporting information). Clinical experiments were approved by the Ethical Committee of the Shanghai Pulmonary Hospital of Tongji University and performed in accordance with the ethical standards. Fig. 4a shows ΔI_{Cd} obtained from different clinical samples and Fig. 4b further displays the violin plots of ΔI_{Cd} obtained in the three groups. The average ΔI_{Cd} (1.52 μA) in lung cancer patients was a bit higher than that in the healthy controls (1.36 μA). But, the average ΔI_{Cd} in the patients at the early stage (I&II) (1.54 μA) was almost as same as that at the advanced stage (III&IV) (1.51 μA). Thus, electrochemical mea-

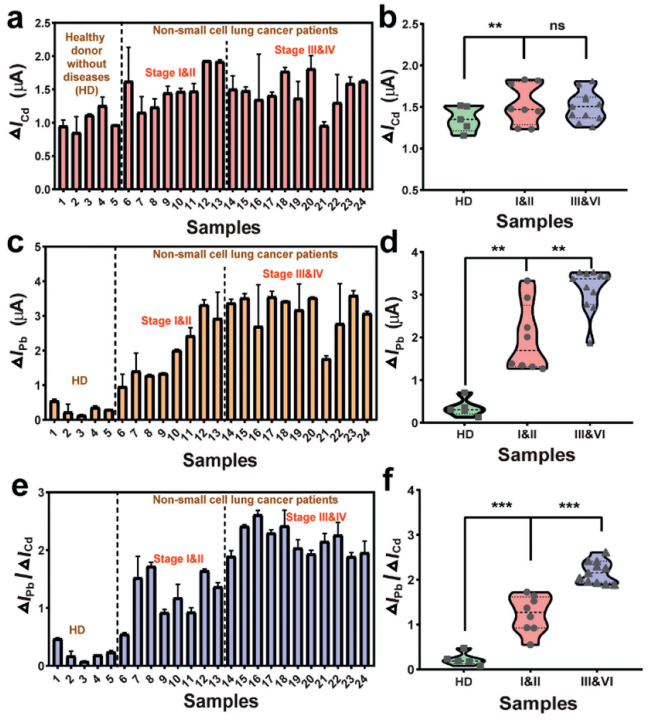

Fig. 4. (a) ΔI_{Cd} and (b) violin plots of ΔI_{Cd} obtained in the clinical samples from healthy donors without diseases (HD) and patients diagnosed with non-small cell lung cancer at the early stages (Stage I&II) and the advanced stages (Stage III&IV). (c) ΔI_{Pb} and (d) violin plots of ΔI_{Pb} obtained in the clinical samples. (e) $\Delta I_{Pb}/\Delta I_{Cd}$ and (f) violin plots of $\Delta I_{Pb}/\Delta I_{Cd}$ obtained in the clinical samples. In (b), (d), and (f), statistical significance was calculated by two-tailed Student's *t*-test; ns, nonsignificant; $^{**}P < 0.01$; $^{***}P < 0.001$.

surements using ΔI_{Cd} suggested that total exosome concentration was able to distinguish lung cancer patients from healthy people, but failed in tumor staging. Figs. 4c and d display the ΔI_{Pb} obtained from different clinical samples. Obviously, the average ΔI_{Pb} was able to distinguish non-small cell lung cancer patients (2.64 μA) from healthy donors (0.36 μA), and also increased as the disease progression (1.98 μA for the early stages versus 3.10 μA for the advanced stages). Nevertheless, the overlap of the distributions for different groups indicated that the tumor classification using only ΔI_{Pb} was still difficult for poor accuracy. Hence, the ratiometric signal, $\Delta I_{Pb}/\Delta I_{Cd}$, was recruited to examine the clinical samples. Figs. 4e and f show the values and violin plots of $\Delta I_{Pb}/\Delta I_{Cd}$ obtained from the serum samples. The low average value of 0.227 was calculated for controls, and higher average value of 1.23 and 2.17 were accounted for patients at the early stages and the advanced stages, respectively. Statistical analysis demonstrated that the average values of $\Delta I_{Pb}/\Delta I_{Cd}$ for lung cancer patients were significantly higher than that for healthy controls, and the distribution of violin plots was in relatively narrow ranges and displayed improved significance difference between patients at the early and advanced stages, which was ascribed to the elimination of individual differences in total exosome concentration. Seven of the non-small cell lung cancer patients participating in the work (Nos. 12, 13, 14, 16, 18, 20, and 24) underwent PD-L1 immunohistochemistry (IHC) tests in the hospital and their PD-L1 IHC scores and $\Delta I_{Pb}/\Delta I_{Cd}$ values were listed in Table S3 (Supporting information). It could be found that there was a good agreement between the two results, revealing the potential of our method in the diagnosis of non-small cell lung cancer and the identification of therapeutic targets. In addition, the method was applied to analyze serum samples from patients diagnosed with non-metastatic breast cancer at the early stages ($n = 5$). As shown in Fig. S20 (Supporting in-

formation), the obtained $\Delta I_{Pb}/\Delta I_{Cd}$ values were significantly lower than those for non-small cell lung cancer patients at the early stages, demonstrating the good selectivity of our method.

In conclusion, we reported a dual-labelled electrochemical method to evaluate the lung cancer-derived exosomes by eliminating the individual differences in the total amount of circulating exosomes. Cholesterol-modified DNA probe inserted into the exosome membrane and provided a quantitative signal for total exosome. At the meanwhile, an antibody-nucleic acid probe selectively bound to the exosomal PD-L1 and offered another quantitative signal. Both the signals allowed the quantification of lung cancer-derived exosomes with desirable detection limits of 826 particles/mL and 985 particles/mL. However, the two signals still faced challenges when used to analyze lung cancer-derived exosomes in clinical samples. In this regard, a ratiometric signal, $\Delta I_{Pb}/\Delta I_{Cd}$, was recruited to reflect the variation in PD-L1 expression at total exosome level, and demonstrated the feasibility in the clinical diagnosis and staging of non-small cell lung cancer patients with improved accuracy. Compared to conventional quantification of total exosome using one quantitative signal, the monitoring of relative PD-L1-expressing level took into account the combined effects of both exosome and protein differences among individuals, and was essential for the elaboration of targeted therapeutic plans aiming to the disease development. Therefore, dual-labelled analysis of lung cancer-derived exosomes may provide precise information for early screening, staging and prognosis of lung cancer, and also guide the individual treatments by revealing specific therapeutic targets.

Declaration of competing interest

The authors declare that they have no known competing financial interests or personal relationships that could have appeared to influence the work reported in this paper.

CRediT authorship contribution statement

Lingjun Sha: Writing – original draft, Methodology, Investigation. **Bing Bo:** Writing – original draft, Methodology, Investigation. **Jiayu Li:** Writing – original draft, Investigation. **Qi Liu:** Investigation. **Ya Cao:** Writing – review & editing, Supervision, Methodology. **Jing Zhao:** Writing – review & editing, Supervision, Conceptualization.

Acknowledgments

This work was supported by the National Natural Science Foundation of China (Nos. 81972799, 82202834, and 81871449).

Supplementary materials

Supplementary material associated with this article can be found, in the online version, at doi:10.1016/j.cclet.2024.110109.

References

[1] J. Ferlay, M. Colombet, I. Soerjomataram, et al., Int. J. Cancer 149 (2021) 778–789.
[2] J.K. Field, M. Oudkerk, J.H. Pedersen, S.W. Duffy, Lancet 382 (2013) 732–741.
[3] A. Ruano-Ravina, M. Pérez-Ríos, P. Casàn-Clará, M. Provencio-Pulla, Lancet Oncol. 19 (2018) e131–e132.
[4] J. Qiu, J. Xu, K. Zhang, et al., Theranostics 10 (2020) 2374.
[5] C. Rolfo, A. Russo, Nat. Rev. Clin. Oncol. 17 (2020) 523–524.
[6] Y. Zhang, D. Pan, Z. Ning, et al., J. Nanobiotechnol. 21 (2023) 467.
[7] Y. Chen, H. Chen, C. Yang, et al., Chin. Chem. Lett. 34 (2023) 107352.
[8] S. Cui, Z. Cheng, W. Qin, L. Jiang, Lung Cancer 116 (2018) 46–54.
[9] F.I.D. Dimtrakopoulos, A. Kottorou, A. Yang, et al., J. Clin. Oncol. 34 (2016) e23016.
[10] H. Zheng, Y. Zhan, S. Liu, et al., J. Exp. Clin. Cancer Res. 37 (2018) 226.
[11] S. Lin, Z. Yu, D. Chen, et al., Small 16 (2020) 1903916.
[12] M. Mohammadi, H. Zargartalebi, R. Salahandish, et al., Biosens. Bioelectron. 183 (2021) 113176.
[13] H. Shin, S. Oh, S. Hong, et al., ACS Nano 14 (2020) 5435–5444.
[14] H. Xiong, Z. Huang, Z. Yang, et al., Small 17 (2021) 2007971.
[15] Y. Lu, Z. Tong, Z. Wu, et al., Chin. Chem. Lett. 33 (2022) 3188–3192.
[16] Q. Yang, L. Cheng, L. Hu, et al., Biosens. Bioelectron. 163 (2020) 112290.
[17] G. Chen, A.C. Huang, W. Zhang, et al., Nature 560 (2018) 382–386.
[18] C. Li, C. Li, C. Zhi, et al., J. Transl. Med. 17 (2019) 355.
[19] Y. Pang, J. Shi, X. Yang, et al., Biosens. Bioelectron. 148 (2020) 111800.
[20] P. Chidchob, D. Offenbartl-Stiegert, D. McCarthy, et al., J. Am. Chem. Soc. 141 (2019) 1100–1108.
[21] J.Y. Kishi, T.E. Schaus, N. Gopalkrishnan, F. Xuan, P. Yin, Nat. Chem. 10 (2018) 155–164.
[22] R. Huang, L. He, Y. Xia, et al., Small 15 (2019) 1900735.
[23] P. Miao, X. Ma, L. Xie, et al., Nano Energy 92 (2022) 106781.
[24] X. Liu, X. Gao, L. Yang, Y. Zhao, F. Li, Anal. Chem. 93 (2021) 11792–11799.
[25] Z. Sun, L. Wang, S. Wu, et al., Anal. Chem. 92 (2020) 3819–3826.
[26] L. Wang, Y. Deng, J. Wei, et al., Biosens. Bioelectron. 191 (2021) 113465.
[27] Y. Cao, L. Li, B. Han, et al., Biosens. Bioelectron. 141 (2019) 111397.
[28] J. Zhang, J. Chen, Q. Xie, et al., Sensors Actuat. B: Chem. 393 (2023) 134273.
[29] D. Pan, Y. Lin, X. Liu, et al., Biosens. Bioelectron. 217 (2022) 114705.
[30] M. Zhang, T. Zhang, W. Mei, et al., Sensors Actuat. B: Chem. 404 (2024) 135252.
[31] R. Kim, B. Mun, S. Lim, et al., Small 20 (2024) 2307262.
[32] J. Chen, J. Guo, M. Hu, et al., Sensors Actuat. B: Chem. 409 (2024) 135614.
[33] L. Yang, H. Guo, T. Hou, et al., Chin. Chem. Lett. 34 (2023) 107607.